
Since January 2020 Elsevier has created a COVID-19 resource centre with free information in English and Mandarin on the novel coronavirus COVID-19. The COVID-19 resource centre is hosted on Elsevier Connect, the company's public news and information website.

Science of the Total Environment 739 (2020) 140000

Contents lists available at ScienceDirect

Science of the Total Environment

journal homepage: www.elsevier.com/locate/scitotenv

# Significant changes in the chemical compositions and sources of $PM_{2.5}$ in Wuhan since the city lockdown as COVID-19

Huang Zheng [a,b], Shaofei Kong [a,d,*], Nan Chen [c,d], Yingying Yan [a,d], Dantong Liu [e], Bo Zhu [c,d], Ke Xu [c,d], Wenxiang Cao [c,d], Qingqing Ding [c,d], Bo Lan [c,d], Zhouxiang Zhang [c,d], Mingming Zheng [b,c], Zewei Fan [b], Yi Cheng [a], Shurui Zheng [a,b], Liquan Yao [a,b], Yongqing Bai [f], Tianliang Zhao [g], Shihua Qi [b,d]

[a] Department of Atmospheric Sciences, School of Environmental Studies, China University of Geosciences, Wuhan 430074, China
[b] Department of Environmental Science and Engineering, School of Environmental Studies, China University of Geosciences, Wuhan 430074, China
[c] Eco-Environmental Monitoring Centre of Hubei Province, Wuhan 430072, China
[d] Research Centre for Complex Air Pollution of Hubei Province, Wuhan, China
[e] Department of Atmospheric Sciences, School of Earth Sciences, Zhejiang University, Hangzhou 310058, China
[f] Hubei Key Laboratory for Heavy Rain Monitoring and Warning Research, Institute of Heavy Rain, China Meteorological Administration, Wuhan 430205, China
[g] School of Atmospheric Physics, Nanjing University of Information Science and Technology, Nanjing 210044, China

## HIGHLIGHTS

- Differences in $PM_{2.5}$ chemical species and sources since lockdown were reported.
- Primary emission reduced while secondary formation enhanced since lockdown.
- Emission reduction dominated the improvement of air quality in Wuhan during lockdown.

## GRAPHICAL ABSTRACT

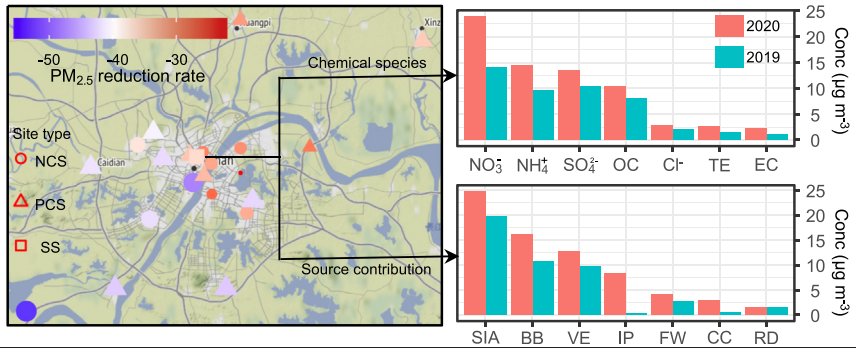


## ARTICLE INFO

*Article history:*
Received 11 May 2020
Received in revised form 2 June 2020
Accepted 3 June 2020
Available online 5 June 2020

*Keywords:*
COVID-2019
Fine particle
Chemical composition
Source apportionment
Random forest tree
Regional transportation

## ABSTRACT

Wuhan was the first city to adopt the lockdown measures to prevent COVID-19 spreading, which improved the air quality accordingly. This study investigated the variations in chemical compositions, source contributions, and regional transport of fine particles ($PM_{2.5}$) during January 23–February 22 of 2020, compared with the same period in 2019. The average mass concentration of $PM_{2.5}$ decreased from 72.9 μg $m^{-3}$ (2019) to 45.9 μg $m^{-3}$ (2020), by 27.0 μg $m^{-3}$. It was predominantly contributed by the emission reduction (92.0%), retrieved from a random forest tree approach. The main chemical species of $PM_{2.5}$ all decreased with the reductions ranging from 0.85 μg $m^{-3}$ (chloride) to 9.86 μg $m^{-3}$ (nitrate) ($p < 0.01$). Positive matrix factorization model indicated that the mass contributions of seven $PM_{2.5}$ sources all decreased. However, their contribution percentages varied from −11.0% (industrial processes) to 8.70% (secondary inorganic aerosol). Source contributions of $PM_{2.5}$ transported from potential geographical regions showed reductions with mean values ranging from 0.22 to 4.36 μg $m^{-3}$. However, increased contributions of firework burning, secondary inorganic aerosol, road dust, and vehicle emissions from transboundary transport were observed. This study highlighted the complex and nonlinear response of chemical compositions and sources of $PM_{2.5}$ to air pollution control measures, suggesting the importance of regional-joint control.



* Corresponding author at: Department of Atmospheric Sciences, School of Environmental Studies, China University of Geosciences, Wuhan 430074, China.
*E-mail address:* kongshaofei@cug.edu.cn (S. Kong).

https://doi.org/10.1016/j.scitotenv.2020.140000
0048-9697/

## 1. Introduction

The air quality in China and other countries has improved a lot after the outbreak of the COVID-19 (Sharma et al., 2020; Tobías et al., 2020; Zhang et al., 2020a). For instance, after two weeks of lockdown, the urban air pollutant concentrations in Barcelona markedly decreased by 28– 51% (Tobías et al., 2020). Similarly, the air pollutant concentrations decreased by 18– 43% during the lockdown period compared to previous years in India (Sharma et al., 2020).

In China, the quarantine period began since 2020-01-23 and lasted until the end of February. Due to the restriction measures (Huang et al., 2020) and Spring Festival effects (Kong et al., 2015), many factories were shut down, the traffic volume on roads and construction activities reduced obviously, and the fireworks burning was banned especially in urban regions, etc. The substantial reductions of human activities have reduced the anthropogenic emissions and thus improved the air quality (Fig. S1). Despite obvious emission reductions due to COVID-19, air pollutions still occurred in the North China Plain due to the unfavorable meteorological conditions (Wang et al., 2020). Further research found that the haze events during the lockdown were driven by the enhancement of secondary pollution as the increase of atmospheric oxidizing ability (Huang et al., 2020). Till now, the variations of chemical compositions and local or regional-transported sources of $PM_{2.5}$ were still unclear for the lockdown period.

Previous studies have revealed the role of pollution control measures on air quality improvement (Cai et al., 2017; Kong et al., 2018; Wang et al., 2019; Zheng et al., 2019a). Elemental carbon (EC), organic matter (OM), sulphate, nitrate, and ammonium (SNA) levels in autumn and winter decreased by >50% from 2013 to 2017 in Beijing, due to the implementation of the Air Pollution Prevention Control and Action Plan in China (Wang et al., 2019). Another factor influencing the variations in aerosol compositions and levels is meteorology, which impacts the transportation, dispersion, accumulation, and deposition of air pollutants (Whiteaker et al., 2002; Zhang et al., 2015; Bei et al., 2016). Generally, emission dominates the interannual variability of air pollutants (Chen et al., 2019; Zhai et al., 2019; Zhang et al., 2019a; Zheng et al., 2020), while meteorology dominates the day-to-day variations of them (Zhang et al., 2012; He et al., 2016, 2017). It was estimated that the anthropogenic emission reductions explained 91% of the $PM_{2.5}$ decrease in China from 2013 to 2017 (Zhang et al., 2019a). Meteorology, however, explained >70% variances of daily average pollutant levels over China during 2014 and 2015 (He et al., 2017). The impacts of strictest lockdown measures and meteorology on $PM_{2.5}$ levels, compositions, and sources were still unknown.

This study used the online monitoring datasets to investigate the impacts of lockdown and meteorology on the chemical components and sources of $PM_{2.5}$ for two periods (one-month (01/23– 02/22) since the lockdown of Wuhan in 2020 and the same period in 2019). Positive matrix factorization (PMF) model was adopted to apportion $PM_{2.5}$ sources. A random forest tree method was used to separate the contributions of emission reduction and meteorology to the changes of $PM_{2.5}$ concentrations, chemical species, and sources. A backward trajectory-based method was used to study the impact of regional transport on $PM_{2.5}$ in Wuhan.

## 2. Materials and methods

### 2.1. Observation datasets

Hourly observations of $PM_{2.5}$ chemical compositions including water-soluble ions (WSIs), trace elements (TE), organic carbon (OC), and EC were conducted using on-line instruments during 2020/01/23 00:00 to 2020/02/22: 23:00 at an environmental monitoring supersite in Wuhan. The measurements for the same period in 2019 were also conducted and more details about the instruments were described in Text S1. The site (114.38° E, 30.52° N) is located in the urban center, which is a residential/commercial site, with no obvious industrial emissions at surroundings. Time series of the main chemical species for the two periods are shown in Fig. S2. Additionally, synchronous in-situ observations of six criteria air pollutants (CO, $NO_2$, $O_3$, $PM_{10}$, $PM_{2.5}$, and $SO_2$) were conducted. CO, $NO_x$ ($NO_x = NO + NO_2$), $O_3$, and $SO_2$ were measured with a correlation infrared absorption analyzer (TAPI, model: 300E, USA), a chemiluminescence trace level NO-$NO_2$-$NO_x$ analyzer (Casella, model: ML9841B, UK), an UV photometric $O_3$ analyzer (TEI, model: 49i, USA), and a pulsed UV fluorescence $SO_2$ analyzer (Casella, model: ML9850B, UK), respectively. $PM_{10}$ and $PM_{2.5}$ were measured by an oscillating balance analyzer (TH-2000Z, China) with two separate inlets. Time series of the six criteria air pollutants for the two periods are shown in Fig. S3. In-situ meteorological parameters including ambient temperature (Temp), atmospheric pressure (P), wind speed (WS), wind direction (WD), and relative humidity (RH) are shown in Fig. S4. The mean and standard deviations of air pollutants, chemical compositions, and meteorological parameters for the two periods are listed in Table 1.

### 2.2. De-weather model

The variations of air pollutants are controlled by both meteorological conditions and emissions. To isolate the trend resulted from emissions, an R package "normalweatherr" was used to remove the influence of meteorology (Grange et al., 2018; Vu et al., 2019; Zhang et al., 2020b). The package used a boosted regression tree (RF) approach to model the air pollutant concentrations. The algorithm solved the relationship between air pollutant levels and their predictors including meteorological parameters and time variables such as day of the year (Julian day), day of the week (Monday to Sunday), and hour of a day (0– 23) (Grange et al., 2018). The input dataset was randomly divided into a training dataset (i.e., 70% of input dataset) for constructing the RF model and a testing dataset (30% of input dataset) for testing the performance of the RF model with an unseen dataset. After the building of the RF model, the weather normalized technique was used for predicting the air pollutant level at a certain measured time point (i.e., 2020/01/23 10:00) with randomly selected meteorological parameters for 1000 times. For each prediction, the independent variables (meteorological

**Table 1**
Mean and standard deviation (SD) of the six criteria air pollutants (μg $m^{-3}$), main $PM_{2.5}$ chemical species including water-soluble ions (μg $m^{-3}$), trace elements (ng $m^{-3}$), carbonaceous components (μg $m^{-3}$), and meteorological parameters including ambient temperature (Temp, °C), atmospheric pressure (P, hPa), wind speed (WS, m $s^{-1}$), relative humidity (RH, %), mixing layer height (MLH, m), and solar irradiation (SI, W $m^{-2}$) for the one-month lockdown period of Wuhan in 2020 and the same period in 2019.

| Variables | 2019 | 2020 | Variables | 2019 | 2020 |
|---|---|---|---|---|---|
| | Mean ± SD | Mean ± SD | | Mean ± SD | Mean ± SD |
| CO | 1.02 ± 0.37 | 0.98 ± 0.31 | Fe | 292 ± 235 | 153 ± 135 |
| $NO_2$ | 40.7 ± 28.6 | 18.1 ± 15.6 | Cu | 26.6 ± 28.3 | 11.1 ± 6.48 |
| $O_3$ | 29.7 ± 21.1 | 40.9 ± 18.0 | Zn | 90.2 ± 70.7 | 32.5 ± 24.2 |
| $PM_{10}$ | 76.0 ± 42.4 | 50.4 ± 28.0 | As | 11.8 ± 10.9 | 4.99 ± 4.87 |
| $PM_{2.5}$ | 72.9 ± 35.4 | 45.9 ± 26.9 | Se | 5.00 ± 3.16 | 2.36 ± 2.12 |
| $SO_2$ | 6.15 ± 6.10 | 4.52 ± 3.30 | Ag | 5.80 ± 2.54 | 3.62 ± 2.07 |
| $Na^+$ | 0.21 ± 0.17 | 0.24 ± 0.08 | Cd | 4.11 ± 2.12 | 4.47 ± 2.25 |
| $NH_4^+$ | 14.4 ± 6.65 | 9.59 ± 6.06 | Ba | 78.7 ± 128 | 36.0 ± 55.7 |
| $Mg^{2+}$ | 0.21 ± 0.26 | 0.01 ± 0.01 | Hg | 1.95 ± 0.80 | 1.13 ± 0.87 |
| $K^+$ | 2.02 ± 2.13 | 1.22 ± 1.11 | Pb | 47.7 ± 36.8 | 17.3 ± 12.1 |
| $Ca^{2+}$ | 0.48 ± 0.39 | 0.08 ± 0.10 | OC | 10.4 ± 4.21 | 8.09 ± 3.52 |
| $Cl^-$ | 2.82 ± 1.85 | 1.96 ± 1.62 | EC | 2.19 ± 1.23 | 1.15 ± 0.70 |
| $NO_3^-$ | 23.9 ± 12.3 | 14.1 ± 9.49 | Temp | 4.12 ± 3.51 | 8.97 ± 3.90 |
| $SO^2{}_4^-$ | 13.4 ± 6.40 | 10.3 ± 6.48 | P | 1023 ± 5.34 | 1019 ± 5.12 |
| K | 2038 ± 2026 | 1163 ± 1053 | WS | 2.08 ± 1.53 | 0.99 ± 0.79 |
| Ca | 173 ± 222 | 105 ± 104 | RH | 84.3 ± 15.1 | 73.2 ± 19.3 |
| Cr | 2.73 ± 2.44 | 1.28 ± 1.81 | MLH[a] | 318 ± 232 | 415 ± 381 |
| Mn | 23.3 ± 19.3 | 8.17 ± 5.78 | SI[a] | 126 ± 140 | 195 ± 180 |

[a] MLH and SI were derived from the HYSPLIT calculation.

parameters and time variables except for the trend term) were sampled without replacement and were randomly allocated to a dependent variable observation. The meteorologically normalized trend at a specific observation time was then calculated as the arithmetic mean of 1000 predictions. More details about the model can be found elsewhere (https://github.com/skgrange/normalweatherr).

In this study, the RF model was independently applied to the datasets for the study period in 2019 and 2020, respectively. The six criteria air pollutants, main $PM_{2.5}$ chemical species including chloride, sulphate, nitrate, ammonium, trace elements, OC, EC, and source contributions derived from the receptor model (see Section 2.3 and Section 3.3 for details) were meteorologically normalized. The predictors (independent variables) included meteorological parameters (ambient temperature, atmospheric pressure, wind speed, relative humidity, mixing layer height, and solar irradiation) and temporal variables such as an hour of a day, day of a week, and day of a year.

### 2.3. Source apportionment

Positive matrix factorization (PMF 5.0) has been widely used in $PM_{2.5}$ source apportionment (Bressi et al., 2014; Kong et al., 2018; Zheng et al., 2019a; Zhang et al., 2019b). WSIs, OC, EC, and several trace elements were input into the model. Species were grouped into strong, weak, and bad according to their single-noise ratio and percentages below detection limits (Callén et al., 2014; Zheng et al., 2018). The species classification is listed in Table S1. Due to the instrument maintenance or incomplete chemical compositions of $PM_{2.5}$, a small part of samples was excluded from the PMF analysis. Finally, a dataset of 728 (sample) × 21 (species) for 2019 and a dataset of 719 (sample) × 18 (species) for 2020 were input into the PMF model, respectively.

To find the optimal factor number, it was tested from 3 to 9. The diagnostic parameters such as the Pearson correlation coefficient, $Q_{robust}$, and $Q_{true}/Q_{exp}$ were calculated to co-determine the optimal solution. $Q_{true}/Q_{exp}$ is an indicator of the optimal solution that if the factor number is properly estimated, it approaches 1. $Q_{robust}/Q_{true}$ is an indicator of the number of an outlier with scaled residuals larger than 4 and it is equal to 1 when there are no outliers. As shown in Table S2, the Pearson correlation coefficient between the observed and modelled concentrations increased with the factor number increasing, suggesting better fitting results as a large factor number. The $Q_{true}/Q_{exp}$ decreased with the increasing of factor number and it approached 1 for the 7-factor solution. To evaluate the uncertainty associated with random and rotational ambiguity, the bootstrap-displacement (BS-DISP) method was used. In this study, the percentage of cases accepted in BS-DISP decreased with the factor number increasing. The cases accepted in BS-DISP for 7-factor was higher than 6-factor and 8-factor solutions for the dataset in 2020, while it was lower than 6- and 8-factor solutions for the dataset in 2019. To better compare the source apportionment results, 7-factor was considered as the optimal solution. Corresponding results were reported in this study. More details about PMF running and result diagnosis can be found elsewhere (Bressi et al., 2014; Zheng et al., 2018) and in Text S2.

### 2.4. Potential geographical source regions

Hourly backward trajectories reaching the monitoring site were calculated using the HYSPLIT model (Stein et al., 2015) driven by the GDAS_1 reanalysis meteorological field. The start height was set as 100 m above the ground level. 72 h backward air mass trajectories were calculated. The air masses reaching the monitoring site were mainly from north and south directions in this study (Fig. S5). The potential geographical source regions were separated into North China (NC), South China (SC), and Local according to the following procedures: (1) the endpoint with a height >2500 m were excluded due to few impacts of surface emissions on air masses (Kanaya et al., 2016); (2) the endpoints of each trajectory were projected to one of the three regions; (3) the number of trajectory endpoints projected in above regions were counted; (4) the trajectory was classified into SC, NC, and Local in turn, starting with SC because the air masses transported from south direction were less compared to other three regions. If a trajectory spent over 10 h within SC, it was allocated to SC. Similarly, the trajectory was allocated to NC if it spent over 10 h within NC. The air mass was attributed to Local if it spent over 52 h within local areas. This method was used elsewhere (Liu et al., 2019a). The thresholds were somewhat arbitrarily set according to the sensitive analysis of the threshold values on air mass classification and the combination used here showed the best classification (Fig. S6).

### 2.5. Statistical analysis and data visualization

Analysis of variance (ANOVA) was used to test whether the differences of meteorological parameters, chemical compositions, and source contributions for the two periods were significant or not at the 95% confidence interval. Data analysis and visualization were realized by R language (R Core Team, 2018) with packages such as “ggplot2”, “openair”, “lubridate”, “reshap2”, and “normalweatherr”, etc. All these packages can be accessed via the Comprehensive R Archive Network (CRAN: https://cran.r-project.org2).

## 3. Results

### 3.1. Changes in air pollutants

The national mean change rates of CO, $NO_2$, $O_3$, $PM_{10}$, $PM_{2.5}$, and $SO_2$ were −13.0%, −35.7%, 21.9%, −32.5%, −15.0%, and −20.1%, respectively (Fig. S1). The results suggested a substantial improvement of air quality in China during the lockdown period due to COVID-19. Most regions showed a decreasing in $PM_{2.5}$ and an enhancement in $O_3$. The reverse variations of $PM_{2.5}$ and $O_3$ were also reported elsewhere during the lockdown periods (Sharma et al., 2020; Tobías et al., 2020). Previous studies suggested that the $O_3$ increase was related with its enhanced production rate, as the $PM_{2.5}$ reduction impairing its role as a scavenger of hydroperoxy radicals (Li et al., 2019a, 2019b). In this study, the change rates of $NO_2$ (−55.6%), $PM_{10}$ (−33.7%), $PM_{2.5}$ (−37.0%), and $SO_2$ (−26.5%) at the observational site were lower than the national averages of them, suggesting larger impacts of lockdown on air quality in Wuhan.

### 3.2. Variations in chemical compositions

Details about the mass concentrations of measured chemical species for the two periods are listed in Table 1. Fig. 1A and B shows the mass concentrations and percentages of main $PM_{2.5}$ chemical species. SNA were the dominant species, totally accounting for 74.1% and 72.8% of the main chemical compositions of $PM_{2.5}$ in 2019 and 2020, respectively. Compared to those in 2019, the mean mass concentrations of nitrate in 2020 decreased most (9.86 μg $m^{-3}$), followed by ammonium (4.73 μg $m^{-3}$), sulphate (2.90 μg $m^{-3}$), OC (2.22 μg $m^{-3}$), TE (1.17 μg $m^{-3}$), EC (1.02 μg $m^{-3}$), and chloride (0.85 μg $m^{-3}$). The decrease of TE and EC verified the primary emission reduction due to the lockdown of Wuhan city.

The $PM_{2.5}$ chemical compositions associated with air masses from different potential geographical regions for the two periods are compared in Fig. S7. For chemical species associated with local air masses, the mean sulphate level in 2020 ($14.0 \pm 6.19$ μg $m^{-3}$) was higher than that in 2019 ($12.3 \pm 3.85$ μg $m^{-3}$) ($p = 0.82$), while the other species showed reductions compared to 2019. For air masses from NC, the OC and sulphate in 2020 were higher than those in 2019. For other species, they showed lower mass concentrations during the study period in 2020.

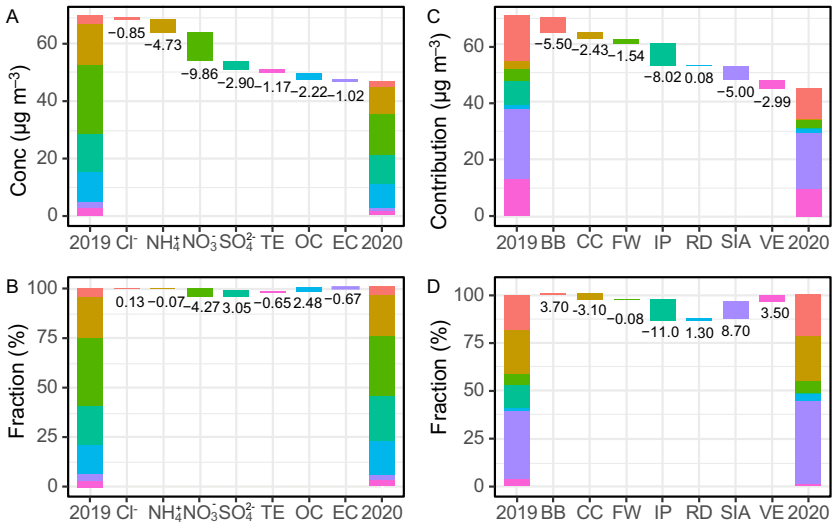


**Fig. 1.** Differences in the main chemical species and source contributions of $PM_{2.5}$ derived from PMF model for the two periods. A and B are the main $PM_{2.5}$ chemical compositions. C and D are PMF source contribution results. BB, CC, FW, IP, RD, SIA, and VE represent biomass burning, coal combustion, firework burning, industrial processes, road dust, secondary inorganic aerosol, and vehicle emissions, respectively.

### 3.3. Variations in source contributions

Seven sources including biomass burning (BB), coal combustion (CC), firework burning (FW), industrial processes (IP), road dust (RD), secondary inorganic aerosol (SIA), and vehicle emissions (VE) were apportioned for both the two periods. Their source profiles and diurnal variations derived from the PMF model are shown in Figs. 2 and 3, respectively. Prior to further analysis, the similarity of the source profiles was checked by Pearson coefficients ($r$), index of agreement (IOA), and coefficient of efficiency (COE). As shown in Table S3, $r$, IOA, and COE varied in the ranges of 0.72– 0.98, 0.54– 0.85, and −0.01– 0.77, respectively. If the source profiles are similar, the $r$, IOA, and COE approach 1. According to this rule, the profiles of BB, CC, RD, SIA, and VE showed high similarity, while the FW and IP showed less similarity. The source identification results were detailedly described as follows.

#### 3.3.1. Biomass burning

$K^+$ is widely used as a tracer of biomass burning (Chen et al., 2017; Zhou et al., 2018; Zheng et al., 2019a). In addition to $K^+$, abundant OC, EC, $Na^+$, $Cl^-$, OC, and EC are also reported for the source profile of biomass burning (Reid et al., 2005), although they vary according to fuel type and combustion efficiency (Bressi et al., 2014). In this study, high loadings of $K^+$ (19.2 ± 6.52% in 2019 and 14.9 ± 15.6% in 2020, the same sequence for the following descriptions) and $Cl^-$ (59.5 ± 15.6% and 72.3 ± 16.1%) were found in this factor. The diurnal variation of this source peaked at noon and night, with lower values occurred at early morning and late afternoon (Fig. 3). Biomass burning was prohibited in urban areas and the source may be related to regional transportation from north China in 2019 and suburban regions of Wuhan in 2020, according to the evidences from conditional probability function (CPF) analysis in Fig. S8. Biomass burning was an important contributor to $PM_{2.5}$ in north China in winter, with the contributions of 7– 12% (Zhang et al., 2013; Shang et al., 2018). In the suburban of Wuhan and its surrounding regions, biomass fuels are still adopted for heating and cooking. Outdoor biomass burning was frequently observed in the surrounding areas of Wuhan (Mehmood et al., 2020). Compared to the same period in 2019, the fire spot numbers detected by MODIS in 2020 reduced (Fig. S9). The contributions of biomass burning also decreased as shown in Fig. 1C.

#### 3.3.2. Coal combustion

High loadings of As (86.2 ± 11.8% and 92.2 ± 8.11%), Se (47.7 ± 10.0% and 42.9 ± 7.51%), and Pb (36.9 ± 10.0% and 38.8 ± 4.96%) were found in this factor, which have been widely reported as the tracers of coal combustion (Tian et al., 2015; Liu et al., 2018; Zhou et al., 2018; Liu et al., 2019b). Additionally, this factor was positively correlated with $SO_2$ ($r = 0.65$, $p < 0.01$ for 2019 and $r = 0.52$, $p < 0.01$ for 2020). Therefore, it was reasonable to attribute this factor to coal combustion.

#### 3.3.3. Firework burning

Firework burning was characterized by high loadings on K (49.5 ± 4.63% and 44.3 ± 5.71%), $K^+$ (49.6 ± 4.38% and 52.3 ± 10.5%), Ba (77.1 ± 6.73% and 68.6 ± 8.26%), and Cu (53.5 ± 6.20% and 39.5 ± 6.34%) (Kong et al., 2015; Rai et al., 2020). $K^+$ was mainly from the furnish paper burning; Cu and Ba were additives for colourful flame (Kong et al., 2015). Higher contributions were found around the New Year's Eve and the Lantern Festival (Fig. S10), with the maximum contributions occurring at ~02:00. Firework burning is prohibited in the urban areas of Wuhan. The high contributions of this source occurred with wind speed higher than 3 m $s^{-1}$ (Fig. S8). Therefore, this factor was attributed to firework burning and it was mainly associated with regional transportation.

#### 3.3.4. Industrial processes

This factor was characterized by high loadings on Cr (43.9 ± 23.7% and 91.9 ± 23.1%), Mn (48.8 ± 16.8% and 21.3 ± 4.92%), Fe (33.5 ± 11.5% and 25.5 ± 6.02%), and Zn (27.9 ± 10.4% and 15.5 ± 2.75%) (Taiwo et al., 2014). $PM_{2.5}$ emitted from iron and steel industry has high fractions of Fe and Mn (An et al., 2015). Cr and Mn are abundant in particles from stainless steel production and Zn is abundant for particles emitted from Zn metallurgy emissions (Querol et al., 2007). This factor can be attributed to local industrial processes in Wuhan. It was verified by the high CPF values under low wind speed (i.e., <1 m $s^{-1}$) in east (2019) and south directions (2020) (Fig. S8), where locates plenty of industrial plants (Fig. S11). Two peak contributions at daytime and lower contributions at night of this factor in 2019 were also related to the daily production activities of industrial processes (Merico et al., 2020).

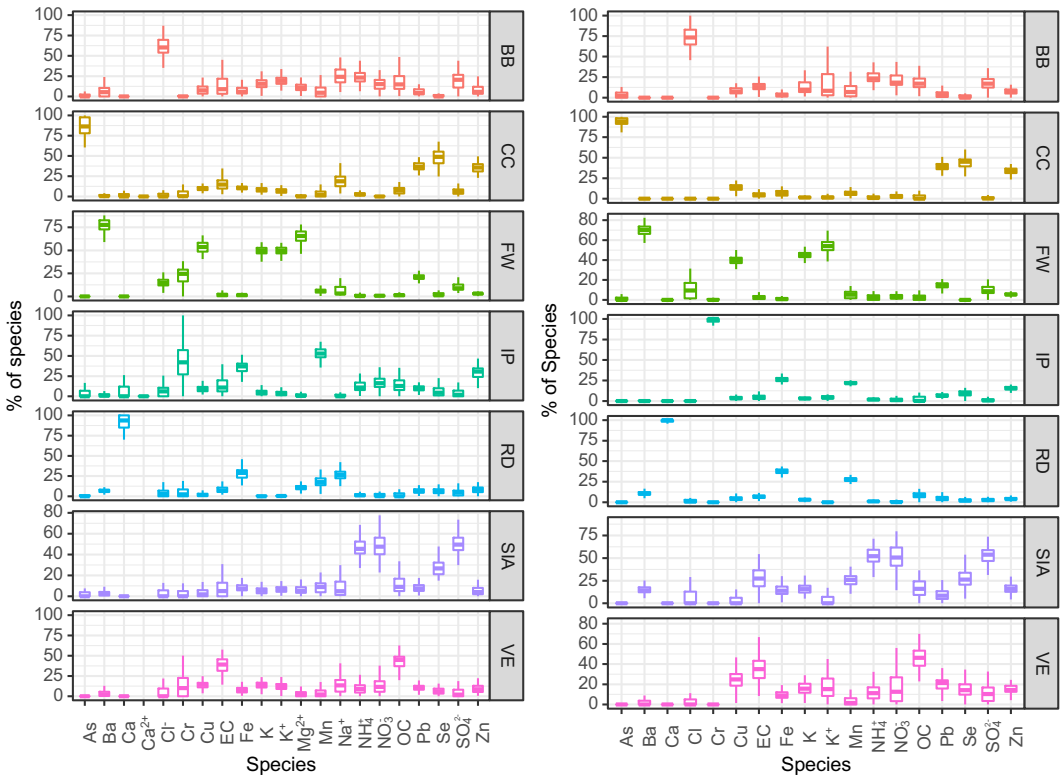


**Fig. 2.** Source profiles of biomass burning (BB), coal combustion (CC), firework burning (FW), industrial processes (IP), road dust (RD), secondary inorganic aerosol (SIA), and vehicle emissions (VE) for 01/23 00:00– 02/22 23:00 in 2019 (left panel) and 2020 (right panel) derived from PMF model. The boxplots are constructed according to the bootstrap results (n = 100).

*3.3.5. Road dust*

This factor was highly loaded on crustal elements, like Ca (91.6 ± 8.21% and 94.9 ± 13.0%), Fe (29.5 ± 8.30%, and 37.6 ± 6.43%), and Mn (20.1 ± 12.4% and 27.7 ± 6.04%). A previous study conducted in Wuhan identified a similar source as fugitive dust due to high loadings on Ba, Ca, Fe, and Mn (Lyu et al., 2016). Fe and Mn are also abundant in brake wear and tyre wear dusts (Garg et al., 2000; Adachi and Tainosho, 2004). According to these markers, road dust was widely identified around the world (Richard et al., 2011; Pancras et al., 2013; Tao et al., 2014; Waked et al., 2014; Lyu et al., 2016; Liu et al., 2019b). Therefore, this factor was identified as road dust in this study.

*3.3.6. Secondary inorganic aerosol*

$SO^{2-}_4$ (50.6 ± 9.60% and 52.2 ± 10.8%), $NO^{-}_3$ (47.3 ± 11.6% and 50.9 ± 15.0%), and $NH^{+}_4$ (46.8 ± 8.76% and 51.5 ± 10.3%) had higher loadings on this factor (Lyu et al., 2016; Zhang et al., 2013; Zheng et al.,

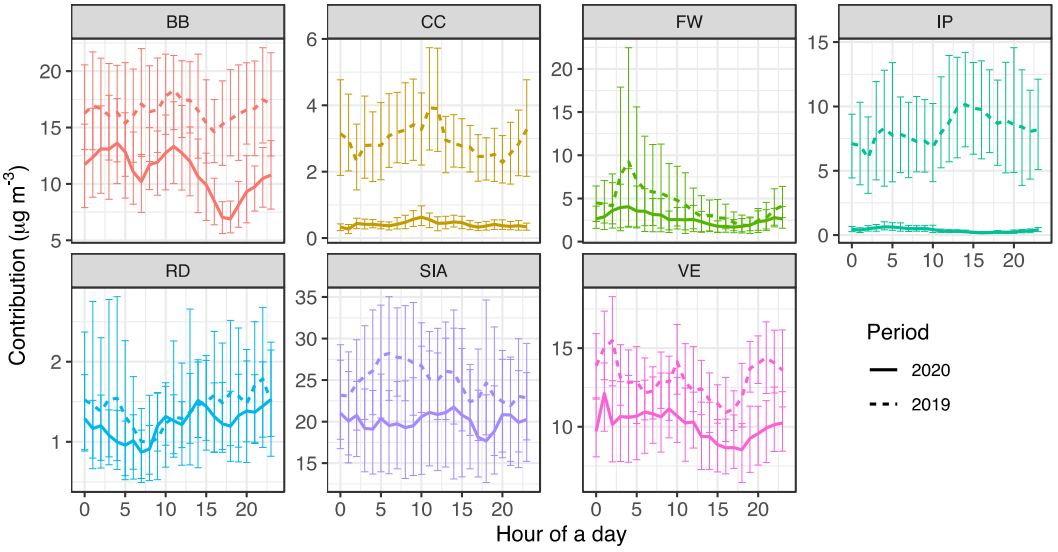


**Fig. 3.** Diurnal variations of seven $PM_{2.5}$ sources derived from the PMF model during 01/23 0:00– 02/22 23:00 in 2019 (dashed line) and 2020 (solid line). The error bars represent the 95% confidence intervals of the mean.

2019a). Excepted for their primary emissions from coal combustion (Dai et al., 2018; Zhang et al., 2018; Yan et al., 2020), SIA can be formed from the atmospheric homogenous and heterogeneous reactions of their precursors (Seinfeld and Pandis, 2006). As shown in Fig. S8, high contributions of this factor were found for both low and high wind speeds, which favoured their formation locally or through regional transportation.

*3.3.7. Vehicle emissions*

This factor had higher loadings on OC (41.7 ± 12.1% and 45.7 ± 11.5%) and EC (37.5 ± 12.9% and 34.5 ± 6.21%) and moderate loadings on Cu (13.8 ± 3.79%, 23.0 ± 10.5%) and Pb (10.4 ± 3.59% and 19.6 ± 7.66%). A similar factor was resolved in previous studies, which was identified as vehicle emissions (Xia and Gao, 2011; Yao et al., 2016; Liu et al., 2018; Zheng et al., 2019a). Significant positive correlations ($r = 0.39$, $p < 0.001$ in 2019 and $r = 0.35$, $p < 0.001$ in 2020) between this factor and $NO_2$ were found. Additionally, the diurnal variations showed morning and evening peaks in 2019, which reflected the daily variation of traffic activities. The diurnal pattern of this source in 2020 was not as clear as that in 2019, which should be related to the prohibition running of private cars during the city lockdown period (Fig. 3).

The mass concentrations and percentages of the seven sources are shown in Fig. 1C and D. The top three contributors to $PM_{2.5}$ mass were SIA, BB, and VE. Industrial processes exhibited the highest reduction of mass concentration contribution (8.02 μg $m^{-3}$), followed by BB (5.50 μg $m^{-3}$), SIA (5.00 μg $m^{-3}$), VE (2.99 μg $m^{-3}$), CC (2.43 μg $m^{-3}$), and FW (1.54 μg $m^{-3}$). The percentage contributions of CC, IP, and FW also showed reductions of 3.10%, 11.0%, and 0.08%, respectively, while the percentage contribution of SIA increased by 8.70%. The reverse variations of these sources suggested the decreased primary emissions but enhanced secondary formation rate during the lockdown.

The diurnal variations of $PM_{2.5}$ source contributions showed differences for the two periods (Fig. 3). For industrial processes, it showed double peaks in 2019 while it monotonically decreased from about 05:00 to 16:00 during the study period in 2020. The diurnal variation of VE indicated that the peak value at 10:00 (local time) in 2020 was impaired compared to 2019. Previous studies concerning the impacts of short-term pollution control measures for mega-events on air pollutant variations showed decreases of air pollutants, while the diurnal patterns of air pollutants during control period were similar to the non-control period (Wang et al., 2015; Liu et al., 2015, 2017). The results here implied that the strictest lockdown measures not only reduced the primary emissions obviously but also changed the diurnal variation patterns of air pollutants. The universal reductions of air pollutants from various sources indicated a possibility of precise control of $PM_{2.5}$ at a specific time of a day.

Fig. S7 shows the mean $PM_{2.5}$ source contributions associated with different air mass classifications. For local air masses, the SIA mass contributions in 2020 (25.5 ± 12.8 μg $m^{-3}$) were higher than that in 2019 (17.5 ± 12.5 μg $m^{-3}$), while other sources showed obvious decreases compared to 2019. For air masses from NC, the mass contributions of the seven sources decreased in 2020 compared with those in 2019. For air masses from SC, the mass contributions of VE (12.7 ± 4.07 μg $m^{-3}$) and RD (1.23 ± 1.07 μg $m^{-3}$) in 2020 were higher than those (10.9 ± 4.65 μg $m^{-3}$ for VE and 0.57 ± 0.57 μg $m^{-3}$ for RD) in 2019.

## 4. Discussions

### 4.1. Role of emission on reduction

As shown in Table 1, higher ambient temperature, mixing layer height, solar irradiation, lower relative humidity, and wind speed in 2020 compared with those for 2019 were found. Due to the conflicting roles of these meteorological conditions on air pollutant formation and removal processes (Zhang et al., 2015; Chen et al., 2020), it was difficult to discuss the influences of emission reduction on air pollutant concentrations. Therefore, a weather normalized technic was adopted to analyze the influence of emission on air pollutant variations. After the weather normalized procedures, the pollutant levels can represent the anthropogenic emissions (Li et al., 2019a; Zhai et al., 2019). The differences between the observed and de-weather levels of air pollutants can be regarded as meteorology related variations. As shown in Fig. S12, meteorological conditions were favorable for reducing air pollutant concentrations for both the two periods. The pollutant emission dominated the reduction of air pollutants during the study period of 2019 and 2020 (Fig. 4).

The observed $PM_{2.5}$ decreased by 27.0 μg $m^{-3}$ in the study period of 2020 (45.9 μg $m^{-3}$), compared to that of 2019 (72.9 μg $m^{-3}$). The emission reduction contributed to 24.8 μg $m^{-3}$ (92.0%) and meteorology contributed only 2.20 μg $m^{-3}$ (8.00%) to $PM_{2.5}$ decrease. For the main chemical species of $PM_{2.5}$, the variations due to emission were in the range of −0.87 μg $m^{-3}$ ($Cl^-$) to −9.50 μg $m^{-3}$ ($NO^-_3$). Similarly, emission-related variations were −0.37 μg $m^{-3}$ (RD) to −8.09 μg $m^{-3}$ (IP) for $PM_{2.5}$ source contributions. The reduced mass concentrations for air pollutants caused by emission control were higher than those caused by meteorology related variations (Fig. 4). Previous studies suggested that meteorology dominated the day-to-day variations of air pollutants (He et al., 2016, 2017). However, the city lockdown experiment showed that substantial emission reductions dominated the reductions in mass concentrations of $PM_{2.5}$ and its chemical compositions. The air quality improvement is a long-way journey. The results here implicated that air pollution control measures should be continuously taken step by step to improve the air quality in regions with serious air quality issues.

### 4.2. Enhanced contributions from secondary formation

OC, sulphate, nitrate, and ammonium are from both primary emissions and secondary formation (Huang et al., 2014), while EC is from

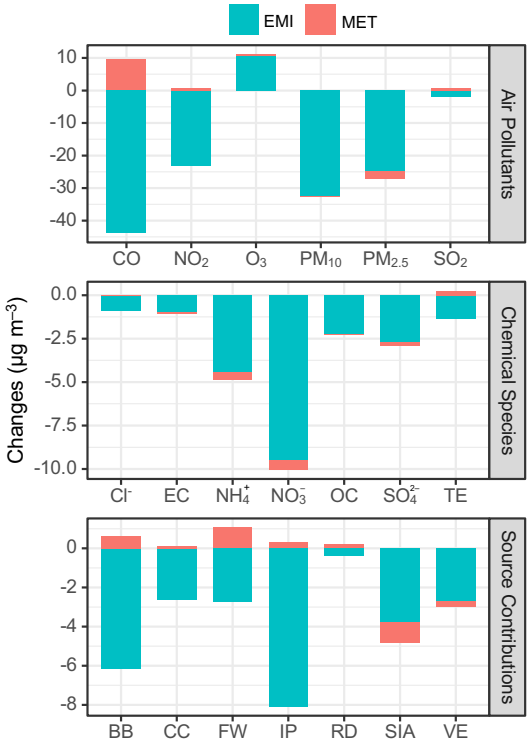


**Fig. 4.** Changes of air pollutants, chemical species, and source contributions of $PM_{2.5}$ between the study period in 2020 and 2019 due to emission (EMI) and meteorology (MET).

primary emissions (Bond et al., 2013; Cao et al., 2013). As shown in Fig. 5, the ratios of OC, sulphate, nitrate, and ammonium for the comparison between 2020 and 2019 were lower than 1, suggesting the reduction of primary emissions in 2020. The atmospheric oxidation ability (AOA), however, enhanced in Wuhan and northern China with the evidence from the increased $O_x$ ($O_3 + NO_2$) (Fig. S1). The ratios of OC, sulphate, nitrate, and ammonium to EC were generally higher than 1 during a day (Fig. 5), suggesting a substantial enhancement of secondary formation (Huang et al., 2020). The sulphate and nitrate oxidation rates (SOR and NOR) also showed enhancements in 2020 (Fig. S13), implying higher fractions of sulphate and nitrate from secondary formation. For OC, sulphate, and ammonium, the ratios to EC ranged from about 5% to ~85% (Fig. 5A, B, D), suggesting stronger formation. The diurnal variations of the scaled sulphate, nitrate, ammonium, and OC (SNAO) by EC for the two periods further showed the enhancement of secondary formation (Fig. S14). The SNAO enhancement from 5:00 to 18:00 coincided with the diurnal cycle of $O_3$, indicating the role of $O_3$ oxidization in secondary formation during the daytime (Brown, 2006; Hallquist et al., 2009).

This unique lockdown experiment can be regarded as an extremely sensitive test of primary emission reduction on air quality. Results here revealed that the primary emission reduced while the secondary formation increased. The lockdown measures yielded a significant decreasing of traffic volumes which subsequently reduced the $NO_x$ levels. Reduction of $NO_x$ emissions is important for $O_3$ and inorganic species controls (South Coast Air Quality Management District, 2013). A recent study suggested that reducing $NO_x$ will reduce nitrate, while increase the secondary organic aerosol (SOA) levels (Zhao et al., 2017) due to the enhancement of AOA (Praske et al., 2018; Huang et al., 2020). The impacts of $NO_x$ reduction on AOA or SOA yield have a tipping-point. Before this tipping-point, reducing $NO_x$ enhances the AOA and promotes the SOA yield, while after this point, further reducing $NO_x$ emissions will impair AOA and limit the yield of SOA (Zhao et al., 2017; Huang et al., 2020). Such significant $NO_x$ reduction during the lockdown still enhanced the AOA in Wuhan. In the short-term, the $NO_x$ emissions will recover in China with the alleviate of COVID-19 (Zhang et al., 2020a) and the AOA should decrease. However, considering the historical decreasing trends of $NO_x$ emission in developed countries (Duncan et al., 2016; Jiang et al., 2018), the $NO_x$ emissions would be decreasing in China continuously. Decreasing volatile organic compounds (VOCs) would offset the secondary formation enhancement as $NO_x$ emission reduction, considering the non-linear relationship between them (Huang et al., 2020). Therefore, further air pollution control would be challenging in China, considering the combination pollution of $PM_{2.5}$ and $O_3$ (Zeng et al., 2019). A two-pollutant strategy to solve $PM_{2.5}$ and ozone problems should be carried out with a focus on VOCs and $NO_x$ emission reduction in further air pollution control policies (Li et al., 2019b).

### 4.3. Reduced emission from different geographical source regions

It was estimated that CO, $NO_x$, $SO_2$, $PM_{2.5}$, BC, and OC emissions decreased by 13–41%, 29–57%, 15–42%, 9–34%, 13–54%, and 3–42%, respectively in the first two months in 2020 compared to 2019 (Huang et al., 2020). The differential concentration-weighted trajectory (DCWT) results (Text S3) showed reductions of source contributions for air masses transported from potential geographical regions affecting Wuhan for the two periods (Fig. 6). Generally, the DCWT values of the seven sources showed negative mean (± standard deviation) values of $-3.29 \pm 6.76$ μg $m^{-3}$ (BB), $-1.28 \pm 1.61$ μg $m^{-3}$ (CC), $-0.26 \pm 3.71$ μg $m^{-3}$ (FW), $-3.87 \pm 5.28$ μg $m^{-3}$ (IP), $-0.22 \pm 0.87$ μg $m^{-3}$ (RD), $-4.36 \pm 11.0$ μg $m^{-3}$ (SIA), and $-2.23 \pm 4.23$ μg $m^{-3}$ (VE), suggesting substantial emission reductions of these sources along the transportation routes to the receptor site. The large standard deviations, however, indicated the spatial variances, especially for BB, FW, and SIA.

The DCWT values of FW increased by 27.5 μg $m^{-3}$ at most for the air masses transported from the eastern Shandong and northern Jiangsu, suggesting the influences of regional transportation of firework burning on air quality in Wuhan, especially for the Spring Festival period. The DCWT values of SIA showed positive values for air masses transported from two routes: central Shanxi and Inner Mongolia as well as the southern Anhui and Jiangsu, with a maximum increase of 30.2 μg $m^{-3}$ and 33.4 μg $m^{-3}$, respectively. The increased DCWT values for SIA

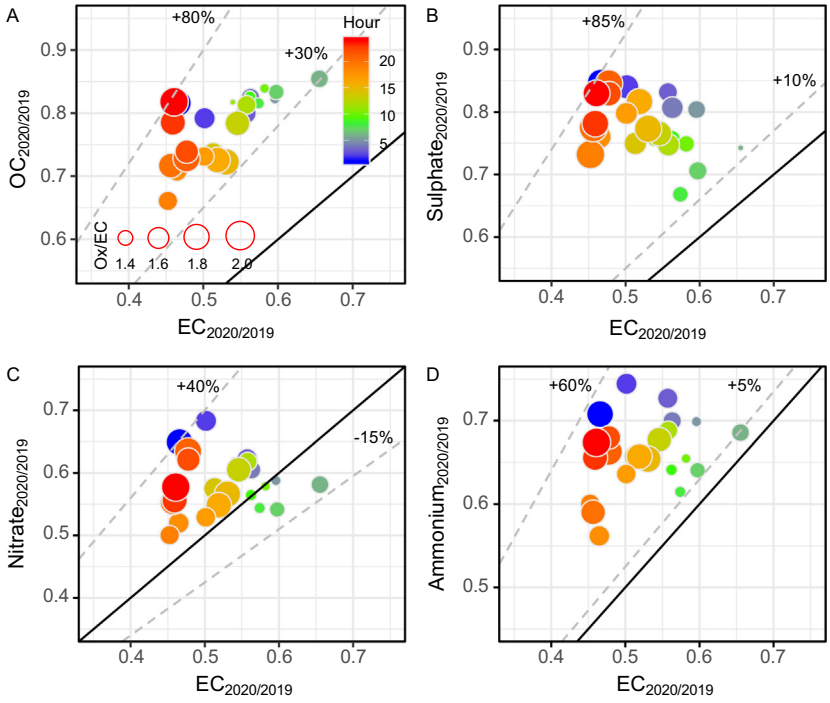


**Fig. 5.** Scatter plots between organic carbon (OC) (A), sulphate (B), nitrate (C), ammonium (D), and elemental carbon (EC) ratios between the observational periods in 2019 and 2020. The colour represents the hour of a day and the dot size represents the scaled levels of $O_x$ ($O_3 + NO_2$) by EC in 2020 to those in 2019. The black solid lines represent the 1:1 ratio and the grey dash lines represent the ranges of ratio changes for the two periods.

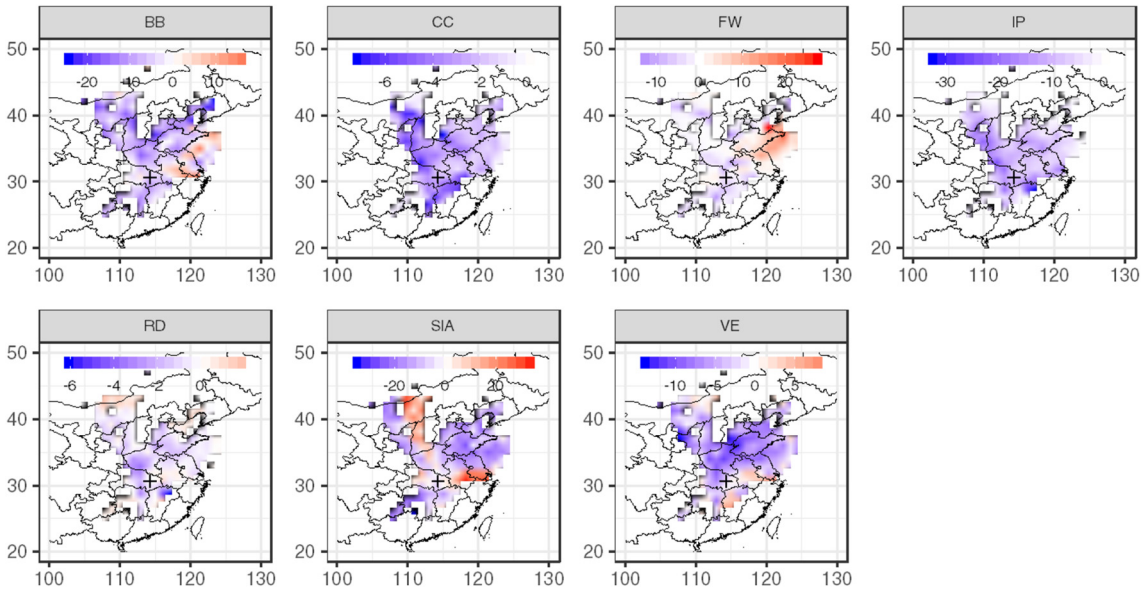


**Fig. 6.** Differential concentration-weighted trajectory (DCWT, μg $m^{-3}$) values of source contributions for the observational period in 2020 compared with those in 2019.

were similar to the results of a recent study that the enhanced secondary formation in the Beijing-Tianjin-Hebei and Yangtze River Delta regions (Huang et al., 2020). The positive DCWT values of SNA scaled by CO, especially for sulphate (Fig. S15) also verified the secondary formation enhancement for the two transport routes.

High $SO_2$ emissions were found in northern China and the lower reach of the Yangtze River (van der A et al., 2017; Kourtidis et al., 2018). The air masses reaching Wuhan during winter were mainly from two transportation routes including north and northeast directions (Zheng et al., 2019b). High emissions and enhanced atmospheric oxidative ability contributed to the secondary formation of sulphate during air mass transportation from the two directions to Wuhan. This phenomenon was further supported by the enhancement of SOR from 0.45 (2019) to 0.68 (2020) for the air masses transported from NC (Fig. S16). The decreased atmospheric oxidative ability (Fig. S1) and less $SO_2$ emissions in south China resulted in less secondary formation of sulphate, which was proved by the reduced SOR from 0.22 (2019) to 0.20 (2020) for air masses transported from SC (Fig. S16).

## 5. Conclusion

In this study, the variations of chemical species and sources of $PM_{2.5}$ in Wuhan were investigated, where the strictest lockdown measures were adopted as COVID-19. Compared to the same period in 2019 (72.9 μg $m^{-3}$), $PM_{2.5}$ levels in the following one month after the lockdown of Wuhan in 2020 (45.9 μg $m^{-3}$) decreased by 27 μg $m^{-3}$, mainly due to the emission reduction (92.0%). The mass concentrations of main $PM_{2.5}$ components showed reductions ranging from 0.85 (chloride) to 9.86 μg $m^{-3}$ (nitrate). The mass contributions of various sources decreased in 1.54 (firework burning)–8.02 μg $m^{-3}$ (industrial processes). The decreases of trace elements (0.65%) and elemental carbon (0.67%) suggested the reduction of primary emissions due to lockdown. The increased mass percentages of sulphate (3.05%), organic carbon (2.48%), and secondary inorganic aerosol (8.70%), however, suggested the enhanced secondary formation of $PM_{2.5}$. The air masses reaching Wuhan from different potential geographical regions showed substantial reductions of the mass contributions from various sources, excepted for biomass burning, firework burning and secondary inorganic aerosols from several regions. This study highlighted that the lockdown measures not only reduced the mass concentrations of air pollutants and associated chemical compositions, but also modified the diurnal variation patterns of $PM_{2.5}$ sources. Further researches should deeply investigate the emission reduction on atmospheric oxidation ability and secondary aerosol formation mechanisms.

## CRediT authorship contribution statement

**Huang Zheng:** Conceptualization, Visualization, Writing - original draft, Writing - review & editing. **Shaofei Kong:** Conceptualization, Funding acquisition, Writing - review & editing, Supervision. **Nan Chen:** Data curation, Resources. **Yingying Yan:** Writing - review & editing. **Dantong Liu:** Writing - review & editing. **Bo Zhu:** Data curation. **Ke Xu:** Data curation. **Wenxiang Cao:** Data curation. **Qingqing Ding:** Data curation. **Bo Lan:** Data curation. **Zhouxiang Zhang:** Data curation. **Mingming Zheng:** Data curation. **Zewei Fan:** Validation. **Yi Cheng:** Validation. **Shurui Zheng:** Writing - review & editing. **Liquan Yao:** Writing - review & editing. **Yongqing Bai:** Conceptualization. **Tianliang Zhao:** Conceptualization. **Shihua Qi:** Resources.

## Declaration of competing interest

The authors declare that they have no known competing financial interests or personal relationships that could have appeared to influence the work reported in this paper.

## Acknowledgements

This study was financially supported by the National Natural Science Foundation of China (41830965), the Key Program of Ministry of Science and Technology of the People's Republic of China (2016YFA0602002 and 2017YFC0212602), the Emergency Research Program for COVID-19 of Wuhan Science and Technology Bureau (2020020201010022), the Key Program for Technical Innovation of Hubei Province (2017ACA089) and the Program for Environmental Protection in Hubei Province (2017HB11). The research was also funded by the Fundamental Research Funds for the Central Universities, China University of Geosciences, Wuhan (G1323519230; 201616; 26420180020; CUG190609) and the Start-up Foundation for Advanced Talents, China University of Geosciences, Wuhan (162301182756). We greatly thank the instrument maintainers, who paid great efforts to keep the equipment running during the tough period.

## Appendix A. Supplementary data

Supplementary data to this article can be found online at https://doi.org/10.1016/j.scitotenv.2020.140000.

## References


Adachi, K., Tainosho, Y., 2004. Characterization of heavy metal particles embedded in tire dust. Environ. Int. 30, 1009–1017. https://doi.org/10.1016/j.envint.2004.04.004.

An, J., Duan, Q., Wang, H., Miao, Q., Shao, P., Wang, J., Zou, J., 2015. Fine particulate pollution in the Nanjing northern suburb during summer: composition and sources. Environ. Monit. Assess. 187. https://doi.org/10.1007/s10661-015-4765-2.

Bei, N., Xiao, B., Meng, N., Feng, T., 2016. Critical role of meteorological conditions in a persistent haze episode in the Guanzhong basin, China. Sci. Total Environ. 550, 273–284. https://doi.org/10.1016/j.scitotenv.2015.12.159.

Bond, T.C., Doherty, S.J., Fahey, D.W., Forster, P.M., Berntsen, T., DeAngelo, B.J., Flanner, M.G., Ghan, S., Kärcher, B., Koch, D., Kinne, S., Kondo, Y., Quinn, P.K., Sarofim, M.C., Schultz, M.G., Schulz, M., Venkataraman, C., Zhang, H., Zhang, S., Bellouin, N., Guttikunda, S.K., Hopke, P.K., Jacobson, M.Z., Kaiser, J.W., Klimont, Z., Lohmann, U., Schwarz, J.P., Shindell, D., Storelvmo, T., Warren, S.G., Zender, C.S., 2013. Bounding the role of black carbon in the climate system: a scientific assessment. J. Geophys. Res. Atmos. 118, 5380–5552. https://doi.org/10.1002/jgrd.50171.

Bressi, M., Sciare, J., Ghersi, V., Mihalopoulos, N., Petit, J.E., Nicolas, J.B., Moukhtar, S., Rosso, A., Féron, A., Bonnaire, N., Poulakis, E., Theodosi, C., 2014. Sources and geographical origins of fine aerosols in Paris (France). Atmos. Chem. Phys. 14, 8813–8839. https://doi.org/10.5194/acp-14-8813-2014.

Brown, S.S., 2006. Variability in nocturnal nitrogen oxide processing and its role in regional air quality. Science 311, 67–70. https://doi.org/10.1126/science.1120120.

Cai, S., Wang, Y., Zhao, B., Wang, S., Chang, X., Hao, J., 2017. The impact of the "Air Pollution Prevention and Control Action Plan" on $PM_{2.5}$ concentrations in Jing-Jin-Ji region during 2012–2020. Sci. Total Environ. 580, 197–209. https://doi.org/10.1016/j.scitotenv.2016.11.188.

Callén, M.S., Iturmendi, A., López, J.M., 2014. Source apportionment of atmospheric $PM_{2.5}$-bound polycyclic aromatic hydrocarbons by a PMF receptor model. Assessment of potential risk for human health. Environ. Pollut. 195, 167–177. https://doi.org/10.1016/j.envpol.2014.08.025.

Cao, J.J., Zhu, C.S., Tie, X.X., Geng, F.H., Xu, H.M., Ho, S.S.H., Wang, G.H., Han, Y.M., Ho, K.F., 2013. Characteristics and sources of carbonaceous aerosols from Shanghai, China. Atmos. Chem. Phys 13, 803–817. https://doi.org/10.5194/acp-13-803-2013.

Chen, J., Li, C., Ristovski, Z., Milic, A., Gu, Y., Islam, M.S., Wang, S., Hao, J., Zhang, H., He, C., Guo, H., Fu, H., Miljevic, B., Morawska, L., Thai, P., Lam, Y.F., Pereira, G., Ding, A., Huang, X., Dumka, U.C., 2017. A review of biomass burning: emissions and impacts on air quality, health and climate in China. Sci. Total Environ. 579, 1000–1034. https://doi.org/10.1016/j.scitotenv.2016.11.025.

Chen, Z., Chen, D., Kwan, M.P., Chen, B., Gao, B., Zhuang, Y., Li, R., Xu, B., 2019. The control of anthropogenic emissions contributed to 80% of the decrease in $PM_{2.5}$ concentrations in Beijing from 2013 to 2017. Atmos. Chem. Phys. 19, 13519–13533. https://doi.org/10.5194/acp-19-13519-2019.

Chen, Z., Chen, D., Zhao, C., Kwan, M., Cai, J., Zhuang, Y., Zhao, B., Wang, X., Chen, B., Yang, J., Li, R., He, B., Gao, B., Wang, K., Xu, B., 2020. Influence of meteorological conditions on $PM_{2.5}$ concentrations across China: a review of methodology and mechanism. Environ. Int. 139, 105558. https://doi.org/10.1016/j.envint.2020.105558.

Dai, Q., Bi, X., Liu, B., Li, L., Ding, J., Song, W., Bi, S., Schulze, B.C., Song, C., Wu, J., Zhang, Y., Feng, Y., Hopke, P.K., 2018. Chemical nature of $PM_{2.5}$ and $PM_{10}$ in Xi'an, China: insights into primary emissions and secondary particle formation. Environ. Pollut. 240, 155–166. https://doi.org/10.1016/j.envpol.2018.04.111.

Duncan, B.N., Lamsal, L.N., Thompson, A.M., Yoshida, Y., Lu, Z., Streets, D.G., Hurwitz, M.M., Pickering, K.E., 2016. A space-based, high-resolution view of notable changes in urban $NO_x$ pollution around the world (2005–2014). J. Geophys. Res. Atmos. 121, 976–996. https://doi.org/10.1002/2015JD024121.

Garg, B.D., Cadle, S.H., Mulawa, P.A., Groblicki, P.J., Laroo, C., Parr, G.A., 2000. Brake wear particulate matter emissions. Environ. Sci. Technol 34, 4463–4469. https://doi.org/10.1021/es001108h.

Grange, S.K., Carslaw, D.C., Lewis, A.C., Boleti, E., Hueglin, C., 2018. Random forest meteorological normalisation models for Swiss PM10 trend analysis. Atmos. Chem. Phys. 18, 6223–6239. https://doi.org/10.5194/acp-18-6223-2018.

Hallquist, M., Wenger, J.C., Baltensperger, U., Rudich, Y., Simpson, D., Claeys, M., Dommen, J., Donahue, N.M., George, C., Goldstein, A.H., Hamilton, J.F., Herrmann, H., Hoffmann, T., Iinuma, Y., Jang, M., Jenkin, M.E., Jimenez, J.L., Kiendler-Scharr, A., Maenhaut, W., McFiggans, G., Mentel, Th.F., Monod, A., Prévôt, A.S.H., Seinfeld, J.H., Surratt, J.D., Szmigielski, R., Wildt, J., 2009. The formation, properties and impact of secondary organic aerosol: current and emerging issues. Atmos. Chem. Phys. 9, 5155–5236. https://doi.org/10.5194/acp-9-5155-2009.

He, J., Yu, Y., Xie, Y., Mao, H., Wu, L., Liu, N., Zhao, S., 2016. Numerical model-based artificial neural network model and its application for quantifying impact factors of urban air quality. Water Air Soil Pollut. 227, 235. https://doi.org/10.1007/s11270-016-2930-z.

He, J., Gong, S., Yu, Y., Yu, L., Wu, L., Mao, H., Song, C., Zhao, S., Liu, H., Li, X., Li, R., 2017. Air pollution characteristics and their relation to meteorological conditions during 2014–2015 in major Chinese cities. Environ. Pollut. 223, 484–496. https://doi.org/10.1016/j.envpol.2017.01.050.

Huang, R.J., Zhang, Y., Bozzetti, C., Ho, K.F., Cao, J.J., Han, Y., Daellenbach, K.R., Slowik, J.G., Platt, S.M., Canonaco, F., Zotter, P., Wolf, R., Pieber, S.M., Bruns, E.A., Crippa, M., Ciarelli, G., Piazzalunga, A., Schwikowski, M., Abbaszade, G., Schnelle-Kreis, J., Zimmermann, R., An, Z., Szidat, S., Baltensperger, U., Haddad, I.E., Prévôt, A.S.H., 2014. High secondary aerosol contribution to particulate pollution during haze events in China. Nature 514, 218–222. https://doi.org/10.1038/nature13774.

Huang, X., Ding, A., Gao, J., Zheng, B., Zhou, D., Qi, X., Tang, R., Ren, C., Nie, W., Chi, X., Wang, J., Xu, Z., Chen, L., Li, Y., Che, F., Pang, N., Wang, H., Tong, D., Qin, W., Cheng, W., Liu, W., Fu, Q., Chai, F., Davis, S.J., Zhang, Q., He, K., 2020. Enhanced secondary pollution offset reduction of primary emissions during COVID-19 lockdown in China (preprint). EarthArXiv https://doi.org/10.31223/osf.io/hvuzy.

Jiang, Z., McDonald, B.C., Worden, H., Worden, J.R., Miyazaki, K., Qu, Z., Henze, D.K., Jones, D.B.A., Arellano, A.F., Fischer, E.V., Zhu, L., Boersma, K.F., 2018. Unexpected slowdown of US pollutant emission reduction in the past decade. Proc. Natl. Acad. Sci. U. S. A. 115, 5099–5104. https://doi.org/10.1073/pnas.1801191115.

Kanaya, Y., Pan, X., Miyakawa, T., Komazaki, Y., Taketani, F., Uno, I., Kondo, Y., 2016. Long-term observations of black carbon mass concentrations at Fukue Island, western Japan, during 2009–2015: constraining wet removal rates and emission strengths from East Asia. Atmos. Chem. Phys. 16, 10689–10705. https://doi.org/10.5194/acp-16-10689-2016.

Kong, S.F., Li, L., Li, X.X., Yin, Y., Chen, K., Liu, D.T., Yuan, L., Zhang, Y.J., Shan, Y.P., Ji, Y.Q., 2015. The impacts of firework burning at the Chinese Spring Festival on air quality: insights of tracers, source evolution and aging processes. Atmos. Chem. Phys. 15, 2167–2184. https://doi.org/10.5194/acp-15-2167-2015.

Kong, S., Yan, Q., Zheng, H., Liu, H., Wang, W., Zheng, S., Yang, G., Zheng, M., Wu, J., Qi, S., Shen, G., Tang, L., Yin, Y., Zhao, T., Yu, H., Liu, D., Zhao, D., Zhang, T., Ruan, J., Huang, M., 2018. Substantial reductions in ambient PAHs pollution and lives saved as a co-benefit of effective long-term $PM_{2.5}$ pollution controls. Environ. Int. 114, 266–279. https://doi.org/10.1016/j.envint.2018.03.002.

Kourtidis, K., Georgoulias, A.K., Mijling, B., van der, A.R., Zhang, Q., Ding, J., 2018. A new method for deriving trace gas emission inventories from satellite observations: the case of $SO_2$ over China. Sci. Total Environ. 612, 923–930. https://doi.org/10.1016/j.scitotenv.2017.08.313.

Li, K., Jacob, D.J., Liao, H., Shen, L., Zhang, Q., Bates, K.H., 2019a. Anthropogenic drivers of 2013–2017 trends in summer surface ozone in China. Proc. Natl. Acad. Sci. U.S.A. 116, 422–427. https://doi.org/10.1073/pnas.1812168116.

Li, K., Jacob, D.J., Liao, H., Zhu, J., Shah, V., Shen, L., Bates, K.H., Zhang, Q., Zhai, S., 2019b. A two-pollutant strategy for improving ozone and particulate air quality in China. Nat. Geosci. 12, 906–910. https://doi.org/10.1038/s41561-019-0464-x.

Liu, Y., Yuan, B., Li, X., Shao, M., Lu, S., Li, Y., Chang, C.C., Wang, Z., Hu, W., Huang, X., He, L., Zeng, L., Hu, M., Zhu, T., 2015. Impact of pollution controls in Beijing on atmospheric oxygenated volatile organic compounds (OVOCs) during the 2008 Olympic Games: observation and modeling implications. Atmos. Chem. Phys. 15, 3045–3062. https://doi.org/10.5194/acp-15-3045-2015.

Liu, Z., Hu, B., Zhang, J., Xin, J., Wu, F., Gao, W., Wang, M., Wang, Y., 2017. Characterization of fine particles during the 2014 Asia-Pacific economic cooperation summit: number concentration, size distribution and sources. Tellus B: Chemical and Physical Meteorology 69, 1303228. https://doi.org/10.1080/16000889.2017.1303228.

Liu, B., Cheng, Y., Zhou, M., Liang, D., Dai, Q., Wang, L., Jin, W., Zhang, L., Ren, Y., Zhou, J., Dai, C., Xu, J., Wang, J., Feng, Y., Zhang, Y., 2018. Effectiveness evaluation of temporary emission control action in 2016 in winter in Shijiazhuang, China. Atmos. Chem. Phys. 18, 7019–7039. https://doi.org/10.5194/acp-18-7019-2018.

Liu, D., Joshi, R., Wang, J., Yu, C., Allan, J.D., Coe, H., Flynn, M.J., Xie, C., Lee, J., Squires, F., Kotthaus, S., Grimmond, S., Ge, X., Sun, Y., Fu, P., 2019a. Contrasting physical properties of black carbon in urban Beijing between winter and summer. Atmos. Chem. Phys. 19, 6749–6769. https://doi.org/10.5194/acp-19-6749-2019.

Liu, D., Joshi, R., Wang, J., Yu, C., Allan, J.D., Coe, H., Flynn, M.J., Xie, C., Lee, J., Squires, F., Kotthaus, S., Grimmond, S., Ge, X., Sun, Y., Fu, P., 2019b. Contrasting physical properties of black carbon in urban Beijing between winter and summer. Atmos. Chem. Phys. 19, 6749–6769. https://doi.org/10.5194/acp-19-6749-2019.

Lyu, X., Chen, N., Guo, H., Zeng, L., Zhang, W., Shen, F., Quan, J., Wang, N., 2016. Chemical characteristics and causes of airborne particulate pollution in warm seasons in Wuhan, central China. Atmos. Chem. Phys. 16, 10671–10687. https://doi.org/10.5194/acp-16-10671-2016.

Mehmood, K., Wu, Y., Wang, L., Yu, S., Li, P., Chen, X., Li, Z., Zhang, Y., Li, M., Liu, W., Wang, Y., Liu, Z., Zhu, Y., Rosenfeld, D., Seinfeld, J.H., 2020. Relative effects of open biomass burning and open crop straw burning on haze formation over central and eastern China: modeling study driven by constrained emissions. Atmos. Chem. Phys. 20, 2419–2443. https://doi.org/10.5194/acp-20-2419-2020.

Merico, E., Grasso, F.M., Cesari, D., Decesari, S., Belosi, F., Manarini, F., De Nuntiis, P., Rinaldi, M., Gambaro, A., Morabito, E., Contini, D., 2020. Characterisation of atmospheric pollution near an industrial site with a biogas production and combustion plant in southern Italy. Sci. Total Environ. 717, 137220. https://doi.org/10.1016/j.scitotenv.2020.137220.

Pancras, J.P., Landis, M.S., Norris, G.A., Vedantham, R., Dvonch, J.T., 2013. Source apportionment of ambient fine particulate matter in Dearborn, Michigan, using hourly resolved PM chemical composition data. Sci. Total Environ. 448, 2–13. https://doi.org/10.1016/j.scitotenv.2012.11.083.

Praske, E., Otkjær, R.V., Crounse, J.D., Hethcox, J.C., Stoltz, B.M., Kjaergaard, H.G., Wennberg, P.O., 2018. Atmospheric autoxidation is increasingly important in urban and suburban North America. Proc. Natl. Acad. Sci. U. S. A. 115, 64–69. https://doi.org/10.1073/pnas.1715540115.

Querol, X., Viana, M., Alastuey, A., Amato, F., Moreno, T., Castillo, S., Pey, J., de la Rosa, J., Sánchez de la Campa, A., Artíñano, B., Salvador, P., García Dos Santos, S., Fernández-Patier, R., Moreno-Grau, S., Negral, L., Minguillón, M.C., Monfort, E., Gil, J.I., Inza, A., Ortega, L.A., Santamaría, J.M., Zabalza, J., 2007. Source origin of trace elements in PM from regional background, urban and industrial sites of Spain. Atmos. Environ. 41, 7219–7231. https://doi.org/10.1016/j.atmosenv.2007.05.022.

R Core Team, 2018. R: A Language and Environment for Statistical Computing. R Foundation for Statistical Computing, Vienna, Austria.

Rai, P., Furger, M., Slowik, J.G., Canonaco, F., Fröhlich, R., Hüglin, C., Minguillón, M.C., Petterson, K., Baltensperger, U., Prévôt, A.S.H., 2020. Source apportionment of highly time-resolved elements during a firework episode from a rural freeway site in Switzerland. Atmos. Chem. Phys. 20, 1657–1674. https://doi.org/10.5194/acp-20-1657-2020.

Reid, J.S., Eck, T.F., Christopher, S.A., Koppmann, R., Dubovik, O., Eleuterio, D.P., Holben, B.N., Reid, E.A., Zhang, J., 2005. A review of biomass burning emissions part III: intensive optical properties of biomass burning particles. Atmos. Chem. Phys. 5, 827–849. https://doi.org/10.5194/acp-5-827-2005.

Richard, A., Gianini, M.F.D., Mohr, C., Furger, M., Bukowiecki, N., Minguillón, M.C., Lienemann, P., Flechsig, U., Appel, K., DeCarlo, P.F., Heringa, M.F., Chirico, R., Baltensperger, U., Prévôt, A.S.H., 2011. Source apportionment of size and time resolved trace elements and organic aerosols from an urban courtyard site in Switzerland. Atmos. Chem. Phys. 11, 8945–8963. https://doi.org/10.5194/acp-11-8945-2011.

Seinfeld, J.H., Pandis, S.N., 2006. Atmospheric Chemistry and Physics: From Air Pollution to Climate Change. 2nd ed. J. Wiley, Hoboken, N.J.

Shang, X., Zhang, K., Meng, F., Wang, S., Lee, M., Suh, I., Kim, D., Jeon, K., Park, H., Wang, X., Zhao, Y., 2018. Characteristics and source apportionment of fine haze aerosol in Beijing during the winter of 2013. Atmos. Chem. Phys. 12.

Sharma, S., Zhang, M., Anshika Gao, J., Zhang, H., Kota, S.H., 2020. Effect of restricted emissions during COVID-19 on air quality in India. Sci. Total Environ. 728, 138878. https://doi.org/10.1016/j.scitotenv.2020.138878.

South Coast Air Quality Management District, 2013. Final 2012 Air Quality Management Plan.

Stein, A.F., Draxler, R.R., Rolph, G.D., Stunder, B.J.B., Cohen, M.D., Ngan, F., 2015. NOAA's HYSPLIT atmospheric transport and dispersion modeling system. Bull. Amer. Meteor. Soc. 96, 2059–2077. https://doi.org/10.1175/BAMS-D-14-00110.1.

Taiwo, A.M., Harrison, R.M., Shi, Z., 2014. A review of receptor modelling of industrially emitted particulate matter. Atmos. Environ. 97, 109–120. https://doi.org/10.1016/j.atmosenv.2014.07.051.

Tao, J., Gao, J., Zhang, L., Zhang, R., Che, H., Zhang, Z., Lin, Z., Jing, J., Cao, J., Hsu, S.C., 2014. $PM_{2.5}$ pollution in a megacity of southwest China: source apportionment and implication. Atmos. Chem. Phys. 14, 8679–8699. https://doi.org/10.5194/acp-14-8679-2014.

Tian, H.Z., Zhu, C.Y., Gao, J.J., Cheng, K., Hao, J.M., Wang, K., Hua, S.B., Wang, Y., Zhou, J.R., 2015. Quantitative assessment of atmospheric emissions of toxic heavy metals from anthropogenic sources in China: historical trend, spatial distribution, uncertainties, and control policies. Atmos. Chem. Phys. 15, 10127–10147. https://doi.org/10.5194/acp-15-10127-2015.

Tobías, A., Carnerero, C., Reche, C., Massagué, J., Via, M., Minguillón, M.C., Alastuey, A., Querol, X., 2020. Changes in air quality during the lockdown in Barcelona (Spain) one month into the SARS-CoV-2 epidemic. Sci. Total Environ. 726, 138540. https://doi.org/10.1016/j.scitotenv.2020.138540.

van der A, R.J., Mijling, B., Ding, J., Koukouli, M.E., Liu, F., Li, Q., Mao, H., Theys, N., 2017. Cleaning up the air: effectiveness of air quality policy for $SO_2$ and $NO_x$ emissions in China. Atmos. Chem. Phys. 17, 1775–1789. https://doi.org/10.5194/acp-17-1775-2017.

Vu, T.V., Shi, Z., Cheng, J., Zhang, Q., He, K., Wang, S., Harrison, R.M., 2019. Assessing the impact of clean air action on air quality trends in Beijing using a machine learning technique. Atmos. Chem. Phys. 19, 11303–11314. https://doi.org/10.5194/acp-19-11303-2019.

Waked, A., Favez, O., Alleman, L.Y., Piot, C., Petit, J.E., Delaunay, T., Verlinden, E., Golly, B., Besombes, J.L., Jaffrezo, J.L., Leoz-Garziandia, E., 2014. Source apportionment of $PM_{10}$ in a north-western Europe regional urban background site (Lens, France) using positive matrix factorization and including primary biogenic emissions. Atmos. Chem. Phys. 14, 3325–3346. https://doi.org/10.5194/acp-14-3325-2014.

Wang, Z., Li, Y., Chen, T., Li, L., Liu, B., Zhang, D., Sun, F., Wei, Q., Jiang, L., Pan, L., 2015. Changes in atmospheric composition during the 2014 APEC conference in Beijing. J. Geophys. Res. Atmos. 120, 12695–12707. https://doi.org/10.1002/2015JD023652.

Wang, Y., Li, W., Gao, W., Liu, Z., Tian, S., Shen, R., Ji, D., Wang, S., Wang, L., Tang, G., Song, T., Cheng, M., Wang, G., Gong, Z., Hao, J., Zhang, Y., 2019. Trends in particulate matter and its chemical compositions in China from 2013–2017. Sci. China Earth Sci. 62, 1857–1871. https://doi.org/10.1007/s11430-018-9373-1.

Wang, Pengfei, Chen, K., Zhu, S., Wang, Peng, Zhang, H., 2020. Severe air pollution events not avoided by reduced anthropogenic activities during COVID-19 outbreak. Resour. Conserv. Recy. 158, 104814. https://doi.org/10.1016/j.resconrec.2020.104814.

Whiteaker, J.R., Suess, D.T., Prather, K.A., 2002. Effects of meteorological conditions on aerosol composition and mixing state in Bakersfield, CA. Environ. Sci. Technol. 36, 2345–2353. https://doi.org/10.1021/es011381z.

Xia, L., Gao, Y., 2011. Characterization of trace elements in $PM_{2.5}$ aerosols in the vicinity of highways in northeast New Jersey in the U.S. east coast. Atmos. Pollut. Res. 2, 34–44. https://doi.org/10.5094/APR.2011.005.

Yan, Q., Kong, S., Yan, Y., Liu, H., Wang, W., Chen, K., Yin, Y., Zheng, H., Wu, J., Yao, L., Zeng, X., Chen, Y., Zheng, S., Wu, F., Niu, Z., Zhang, Y., Zheng, M., Zhao, D., Liu, D., Qi, S., 2020. Emission and simulation of primary fine and submicron particles and water-soluble ions from domestic coal combustion in China. Atmos. Environ. 117308. https://doi.org/10.1016/j.atmosenv.2020.117308.

Yao, L., Yang, L., Yuan, Q., Yan, C., Dong, C., Meng, C., Sui, X., Yang, F., Lu, Y., Wang, W., 2016. Sources apportionment of $PM_{2.5}$ in a background site in the North China Plain. Sci. Total Environ. 541, 590–598. https://doi.org/10.1016/j.scitotenv.2015.09.123.

Zeng, Y., Cao, Y., Qiao, X., Seyler, B.C., Tang, Y., 2019. Air pollution reduction in China: recent success but great challenge for the future. Sci. Total Environ. 663, 329–337. https://doi.org/10.1016/j.scitotenv.2019.01.262.

Zhai, S., Jacob, D.J., Wang, X., Shen, L., Li, K., Zhang, Y., Gui, K., Zhao, T., Liao, H., 2019. Fine particulate matter ($PM_{2.5}$) trends in China, 2013–2018: separating contributions from anthropogenic emissions and meteorology. Atmos. Chem. Phys. 19, 11031–11041. https://doi.org/10.5194/acp-19-11031-2019.

Zhang, J.P., Zhu, T., Zhang, Q.H., Li, C.C., Shu, H.L., Ying, Y., Dai, Z.P., Wang, X., Liu, X.Y., Liang, A.M., Shen, H.X., Yi, B.Q., 2012. The impact of circulation patterns on regional transport pathways and air quality over Beijing and its surroundings. Atmos. Chem. Phys. 12, 5031–5053. https://doi.org/10.5194/acp-12-5031-2012.

Zhang, R., Jing, J., Tao, J., Hsu, S.-C., Wang, G., Cao, J., Lee, C.S.L., Zhu, L., Chen, Z., Zhao, Y., Shen, Z., 2013. Chemical characterization and source apportionment of $PM_{2.5}$ in Beijing: seasonal perspective. Atmos. Chem. Phys. 13, 7053–7074. https://doi.org/10.5194/acp-13-7053-2013.

Zhang, H., Wang, Y., Hu, J., Ying, Q., Hu, X.M., 2015. Relationships between meteorological parameters and criteria air pollutants in three megacities in China. Environ. Res. 140, 242–254. https://doi.org/10.1016/j.envres.2015.04.004.

Zhang, Y., Yuan, Q., Huang, D., Kong, S., Zhang, J., Wang, X., Lu, C., Shi, Z., Zhang, X., Sun, Y., Wang, Z., Shao, L., Zhu, J., Li, W., 2018. Direct observations of fine primary particles from residential coal burning: insights into their morphology, composition, and hygroscopicity. J. Geophys. Res. Atmos. 123. https://doi.org/10.1029/2018JD028988.

Zhang, Q., Zheng, Y., Tong, D., Shao, M., Wang, S., Zhang, Y., Xu, X., Wang, J., He, H., Liu, W., Ding, Y., Lei, Y., Li, J., Wang, Z., Zhang, X., Wang, Y., Cheng, J., Liu, Y., Shi, Q., Yan, L., Geng, G., Hong, C., Li, M., Liu, F., Zheng, B., Cao, J., Ding, A., Gao, J., Fu, Q., Huo, J., Liu, B., Liu, Z., Yang, F., He, K., Hao, J., 2019a. Drivers of improved $PM_{2.5}$ air quality in China from 2013 to 2017. Proc. Natl. Acad. Sci. U. S. A. 116, 24463–24469. https://doi.org/10.1073/pnas.1907956116.

Zhang, Y., Zheng, H., Zhang, L., Zhang, Z., Xing, X., Qi, S., 2019b. Fine particle-bound polycyclic aromatic hydrocarbons (PAHs) at an urban site of Wuhan, central China: characteristics, potential sources and cancer risks apportionment. Environ. Pollut. 246, 319–327. https://doi.org/10.1016/j.envpol.2018.11.111.

Zhang, R., Zhang, Y., Lin, H., Feng, X., Fu, T.M., Wang, Y., 2020a. $NO_x$ emission reduction and recovery during COVID-19 in East China. Atmosphere 11, 433. https://doi.org/10.3390/atmos11040433.

Zhang, Y., Vu, T.V., Sun, J., He, J., Shen, X., Lin, W., Zhang, X., Zhong, J., Gao, W., Wang, Y., Fu, T.M., Ma, Y., Li, W., Shi, Z., 2020b. Significant changes in chemistry of fine particles in wintertime Beijing from 2007 to 2017: impact of clean air actions. Environ. Sci. Technol. 54, 1344–1352. https://doi.org/10.1021/acs.est.9b04678.

Zhao, Y., Saleh, R., Saliba, G., Presto, A.A., Gordon, T.D., Drozd, G.T., Goldstein, A.H., Donahue, N.M., Robinson, A.L., 2017. Reducing secondary organic aerosol formation from gasoline vehicle exhaust. Proc. Natl. Acad. Sci. U. S. A. 114, 6984–6989. https://doi.org/10.1073/pnas.1620911114.

Zheng, H., Kong, S., Xing, X., Mao, Y., Hu, T., Ding, Y., Li, G., Liu, D., Li, S., Qi, S., 2018. Monitoring of volatile organic compounds (VOCs) from an oil and gas station in northwest China for 1 year. Atmos. Chem. Phys. 18, 4567–4595. https://doi.org/10.5194/acp-18-4567-2018.

Zheng, H., Kong, S., Yan, Q., Wu, F., Cheng, Y., Zheng, S., Wu, J., Yang, G., Zheng, M., Tang, L., Yin, Y., Chen, K., Zhao, T., Liu, D., Li, S., Qi, S., Zhao, D., Zhang, T., Ruan, J., Huang, M., 2019a. The impacts of pollution control measures on $PM_{2.5}$ reduction: insights of chemical composition, source variation and health risk. Atmos. Environ. 197, 103–117. https://doi.org/10.1016/j.atmosenv.2018.10.023.

Zheng, H., Kong, S., Wu, F., Cheng, Y., Niu, Z., Zheng, S., Yang, G., Yao, L., Yan, Q., Wu, J., Zheng, M., Chen, N., Xu, K., Yan, Y., Liu, D., Zhao, D., Zhao, T., Bai, Y., Li, S., Qi, S., 2019b. Intra-regional transport of black carbon between the south edge of the North China Plain and central China during winter haze episodes. Atmos. Chem. Phys. 19, 4499–4516. https://doi.org/10.5194/acp-19-4499-2019.

Zheng, H., Kong, S., Zheng, M., Yan, Y., Yao, L., Zheng, S., Yan, Q., Wu, J., Cheng, Y., Chen, N., Bai, Y., Zhao, T., Liu, D., Zhao, D., Qi, S., 2020. A 5.5-year observations of black carbon aerosol at a megacity in Central China: levels, sources, and variation trends. Atmos. Environ. 232, 117581. https://doi.org/10.1016/j.atmosenv.2020.117581.

Zhou, S., Davy, P.K., Huang, M., Duan, J., Wang, X., Fan, Q., Chang, M., Liu, Y., Chen, W., Xie, S., Ancelet, T., Trompetter, W.J., 2018. High-resolution sampling and analysis of ambient particulate matter in the Pearl River Delta region of southern China: source apportionment and health risk implications. Atmos. Chem. Phys. 18, 2049–2064. https://doi.org/10.5194/acp-18-2049-2018.